Chapter 5
Concurrent Backscatter: Enabling Multi-tag to Transmit Concurrently

Abstract The research on backscatter multiple access schemes has been an interesting topic. Existing schemes in the area of backscatter multiple access are not designed for specific applications, and leave out the contemplation of practical application requirements. In this paper, therefore, we present *ConScatter*, a backscatter multiple access scheme that targets indoor Internet of Things (IoT) applications (e.g., the smart home) and considers the practical application requirements. To implement *ConScatter*, we address several key challenges including imperfect time synchronization, high hardware complexity at receiver, and synchronizing multiple tags information in a low-power manner. We theoretically analyze the feasibility of our scheme and evaluate the performance of *ConScatter* through extensive simulations. The results show that *ConScatter* supports concurrent transmissions of up to 7 tags and achieves BER of 0 when SNR is greater or equal to 0 dB.

5.1 Introduction

As a technology for conducting passive communication, backscatter technology [1] has gained significant momentum and is expected to play an increasingly important role in future Internet-of-Things (IoT) applications [2–5]. One potential application scenario is the smart home. In smart homes, backscatter tags can be embedded in objects and environments such as furniture and walls [6]. These tags harvest energy from radio-frequency (RF) signals and modulate and reflect those signals to transmit the collected environmental data (e.g., temperature and humidity) to the decision-making unit [7–14]. In this way, indoor temperature and humidity can be intelligently adjusted by the unit after analyzing those data, thus providing a comfortable living environment for us. Such a vision is depicted in Fig. 5.1.

To realize this vision, the backscatter system should satisfy the following practical requirements.

(1) **Security.** The backscatter system should be resistant to security attacks such as jamming. If the backscatter system is vulnerable to security attacks, the decoded

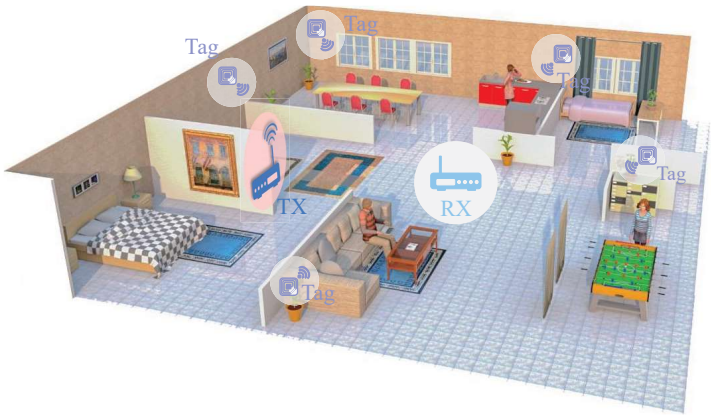

Fig. 5.1 An intelligent and comfortable living environment with the help of backscatter communications.

information may not reflect the real indoor condition, thereby leading to an inhospitable setting.

(2) **Reliability.** The backscattered signal can be corrupted by multipath fading and noise, thereby resulting in a high bit error rate (BER). Therefore, the backscatter system should be resistant to multipath fading and noise owing to the multipath richness in indoor environments.

(3) **Concurrency.** The throughput of the backscatter system is greatly limited by the number of tags that transmits simultaneously. Thus, the backscatter system should support the concurrent transmission from multiple tags to provide a high throughput.

However, to the best of our knowledge, the existing backscatter systems are not designed specifically for indoor applications and rarely consider the above three requirements, as shown in Table 5.1. Netscatter [15] and OFDMA [16] focus on the concurrent transmissions. STScatter [17], HitchHike [18], FreeRider [19], and CAB [20] do not support the simultaneous transmission of multiple tags. Like the studies in [17–20], VMScatter [21] also does not support concurrent transmissions from multiple tags, although it can achieve BER of around 0.000011.

Table 5.1 Summary of existing backscatter systems.

Technology	Security	Reliability	Concurrency
Netscatter [15]		✓	✓
OFDMA [16]		✓	✓
STScatter [17]		✓	
HitchHike [18]		✓	
FreeRider [19]		✓	
CAB [20]		✓	
VMScatter [21]		✓	
ConScatter	✓	✓	✓

The code-division multiple-access (CDMA) mechanism is a potential scheme meeting the requirements above for the following three reasons [22–29].

Reason 1: *CDMA adopts spread spectrum technology, in which the amount of jamming power is spread over the whole bandwidth of the signal. As a result, the jamming has a slight impact on the signal being transmitted, thus satisfying the security requirement.*

Reason 2: *Since the spread-spectrum signal occupies a wide bandwidth, only a small part of the entire signal will be affected by noise and multipath fading, which can be overcome, thus satisfying the reliability requirement.*

Reason 3: *CDMA is a multiple access scheme, where multiple transmitters are able to transmit information simultaneously to a single receiver, thereby satisfying the concurrency requirement.*

Therefore, we propose to design a backscatter multiple access scheme based on CDMA mechanism. The key step in designing such a backscatter scheme is to select the spreading sequence (known as spreading code). In general, spreading sequences can be broadly classified into two main groups: i) orthogonal sequences and ii) non-orthogonal sequences [30]. In contrast to non-orthogonal sequences, orthogonal sequences possess excellent the *orthogonal property*[1]. Owing to the orthogonal property, the interference from other users can be minimized or even eliminated [32], thereby enabling a robust backscatter system that supports simultaneous transmissions from multiple tags. As a result, we present a backscatter multiple access scheme assisted by orthogonal codes, namely *ConScatter*, to achieve the vision depicted in Fig. 5.1. To implement *ConScatter*, we encounter three main challenges.

Challenge 1: How to handle imperfect time synchronization. Ensuring that the signals from different tags reach the receiver simultaneously is quite difficult or even not feasible to achieve in practice [15, 33]. As a result, the orthogonality among sequences can be degraded by imperfect time synchronization, thereby causing a high BER.

Challenge 2: How to handle high hardware complexity on the receiver side. To decode the data transmitted by the ith user, traditional CDMA receivers need to implement a strict synchronization (i.e., providing a *synchronized local carrier*[2] and a *synchronized local code*[3]). However, achieving such synchronization requires a high hardware complexity design, which inevitably results in very high hardware implementation costs, thus limiting the use of *ConScatter*.

Challenge 3: How to synchronize multiple tags information in a low-power manner. If the transmission from tags is arbitrary and random, the orthogonality among orthogonal sequences will be significantly degraded, thereby inducing a large bit error. A potential solution to synchronize multiple tags information is transmitting

---

[1] Code orthogonality between two codes w_i and w_j is defined as that when w_i and w_j are multiplied, the result is summed up over a period of time to zero [31], which is mathematically expressed as: $\int_0^T w_i(t) \cdot w_j(t)dt = 0 \ (i \neq j)$ where T is the spreading code duration and '$\cdot$' denotes the dot product operation.

[2] The local carrier frequency and phase offset in the receiver match that of the incoming signal of the ith user.

[3] The local code and code phase in the receiver match that of the incoming signal of the ith user.

control signals to tags. The problem is how to identify such control signals in a low-power manner on the tag side.
Solutions: Our solutions are as follows.

- We construct a group of novel spreading sequences called *ConScatter* sequences or *ConScatter* codes, which have the ***Property: Any ConScatter code is orthogonal not only to other ConScatter codes, but also to the time-shifted versions of those codes.*** Thus, the orthogonality among *ConScatter* codes can be maintained even under imperfect time synchronization, thereby resolving ***Challenge 1***. With *ConScatter* codes, we can decode the tag data with no need for the local carrier phase offset and the local code phase to match that of the incoming signal, thereby reducing hardware complexity and resolving ***Challenge 2***. The detailed procedures are presented in Section 5.4.4.
- We present a novel excitation signal form, in which the excitation signal is an on-off keying (OOK) modulated signal and comprises two fields, i) *preamble* and ii) *continuous wave*. The preamble is used for triggering the transmissions from multiple tags, which can be identified by using an analog envelope detector and a comparator, thus enabling low-power demodulation at tags.

Contributions. Our main contributions are as follows.

- We illustrate the design of *ConScatter* codes and provide the proof for the *Property* above. More significantly, a backscatter multiple access scheme assisted by *ConScatter* codes is proposed, and the key challenges mentioned above are addressed.
- We theoretically analyze the feasibility of our scheme and evaluate the effectiveness of our scheme through extensive simulations. The results demonstrate that our system achieves BER of 0 when SNR is greater or equal to 0 dB and supports simultaneous transmissions of up to 7 tags.

The rest of this paper is organized as follows. Section 5.2 provides the preliminary knowledge of our work. Section 5.3 describes *ConScatter* sequences. The design of *ConScatter* is presented in Section 5.4. Section 5.5 is devoted to the performance evaluation of *ConScatter*. The related work is given in Section 5.6. Finally, Section 5.7 discusses and concludes this paper.

5.2 Preliminaries

In order to clearly present *ConScatter*, this section will introduce the preliminary knowledge including two aspects, i) spread spectrum and ii) CDMA communications system.

5.2.1 Spread spectrum

Spread spectrum is a technique that is able to convert a signal $x(t)$ with a specific bandwidth into a signal $y(t)$ with a wider bandwidth. This technique is implemented by multiplying $x(t)$ and a spreading code $c(t)$, i.e., $y(t) = x(t)c(t)$. The product of $x(t)$ and $c(t)$ in the time domain is equivalent to the convolution of these two signals in the frequency domain, thereby resulting in $y(t)$ with a wider bandwidth and distributing the power of $x(t)$ over the bandwidth of $y(t)$. As a result, this technique has some significant advantages such as resistance to jamming, interference, and fading. An illustration of resistance to interference is depicted in Fig. 5.2, in which '$*$' denotes the convolution operation. From Fig. 5.2, we can see that the power of

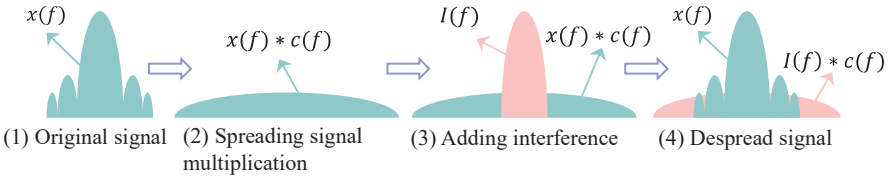

Fig. 5.2 Interference rejection, in which $x(f)$, $c(f)$, and $I(f)$ are signal representations of $x(t)$, $c(t)$, and the interference signal $I(t)$ in the frequency domain, respectively.

the signal $x(t)$ is spread over a relatively wider bandwidth after the spread spectrum operation, and that the despreading operation recovers the power of the signal $x(t)$ and distributes the power of the interference signal $I(t)$ over a large bandwidth. As a result, the interference signal has a slight impact on the signal $x(t)$, which can be overcome.

5.2.2 CDMA communications system

In general, CDMA communications system consists of a group of users and one receiver. Each user is assigned a distinct spreading sequence. Let us consider a CDMA system with k users and each user is assigned a distinct orthogonal sequence denoted by $c_i(t)$, as shown in Fig. 5.3. Assuming that all users transmit at the same power level, then the transmitted signal for the ith user, denoted by $S_i(t)$, can be written as

$$S_i(t) = Ad_i(t)c_i(t)sin(2\pi f_c t) \tag{5.1}$$

where A, $d_i(t)$, $c_i(t)$, and f_c are the signal amplitude, information bits, spreading signal, and carrier frequency for the ith user, respectively.

We illustrate the received signal only for the noise channel. Thus, the received signal at the receiver, denoted by $R(t)$, can be expressed as

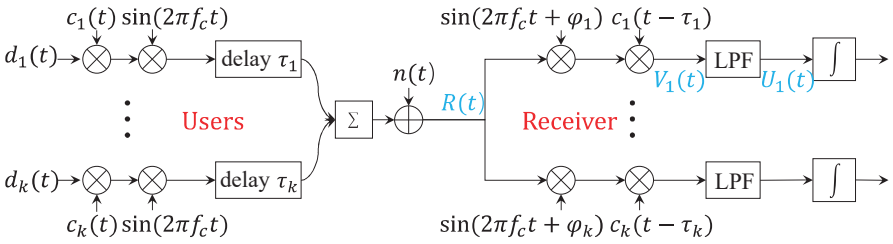

Fig. 5.3 A typical CDMA communications system.

$$\begin{aligned} R(t) &= \sum_{i=1}^{k} A_i d_i(t-\tau_i) c_i(t-\tau_i) sin(2\pi f_c(t-\tau_i)) + n(t) \\ &= \sum_{i=1}^{k} A_i d_i(t-\tau_i) c_i(t-\tau_i) sin(2\pi f_c t + \phi_i) + n(t) \end{aligned} \tag{5.2}$$

where τ_i is the propagation delay from the ith user to the receiver, $\phi_i = -2\pi f_c \tau_i$, A_i is the received signal amplitude from the ith user, and $n(t)$ is an additive white Gaussian noise (AWGN). To decode the data sent by the ith user, the receiver needs to provide a *synchronized local carrier* (i.e., $sin(2\pi f_c t + \phi_i)$) and a *synchronized despreading code* (i.e., $c_i(t-\tau_i)$). After multiplying $R(t)$ by $sin(2\pi f_c t + \phi_i)$ and $c_i(t-\tau_i)$, we obtain

$$\begin{aligned} V_i(t) &= R(t) \times sin(2\pi f_c t + \phi_i) \times c_i(t-\tau_i) \\ &= \left\{ \sum_{i=1}^{k} A_i d_i(t-\tau_i) c_i(t-\tau_i) sin(2\pi f_c t + \phi_i) + n(t) \right\} \\ &\qquad \times sin(2\pi f_c t + \phi_i) \times c_i(t-\tau_i) \\ &= \frac{1}{2} A_i d_i(t-\tau_i) c_i(t-\tau_i) c_i(t-\tau_i)(1 - cos(4\pi f_c t + 2\phi_i)) \\ &\quad + \frac{1}{2} \sum_{\substack{j=1 \\ j \neq i}}^{k} \{ A_j d_j(t-\tau_j) c_j(t-\tau_j) c_i(t-\tau_i) \\ &\qquad \times (cos(\phi_j - \phi_i) - cos(4\pi f_c t + \phi_j + \phi_i)) \} \\ &\quad + n(t) sin(2\pi f_c t + \phi_i) c_i(t-\tau_i) \end{aligned} \tag{5.3}$$

After passing through the low-pass filter (LPF), $V_i(t)$ becomes

$$\begin{aligned} U_i(t) &= \frac{1}{2} A_i d_i(t-\tau_i) c_i(t-\tau_i) c_i(t-\tau_i) \\ &\quad + \sum_{\substack{j=1 \\ j \neq i}}^{k} \frac{1}{2} A_j d_j(t-\tau_j) c_j(t-\tau_j) c_i(t-\tau_i) cos(\phi_j - \phi_i) \end{aligned} \tag{5.4}$$

Suppose that the integrator integrates from τ_i to $\tau_i + T$, where T is one symbol time. The integrator output is then given by

$$\begin{aligned}
&\int_{\tau_i}^{T+\tau_i} U_i(t)dt = \int_{\tau_i}^{T+\tau_i} \frac{1}{2}A_i d_i(t-\tau_i)c_i(t-\tau_i)c_i(t-\tau_i)dt \\
&+\int_{\tau_i}^{T+\tau_i} \sum_{\substack{j=1 \\ j\neq i}}^{k} \frac{1}{2}A_j d_j(t-\tau_j)c_j(t-\tau_j)c_i(t-\tau_i)cos(\phi_j-\phi_i)dt \\
&\approx \frac{1}{2}A_i T d_i + \frac{1}{2}\sum_{\substack{j=1 \\ j\neq i}}^{k} \int_{\tau_i}^{T+\tau_i} \{A_j d_j(t-\tau_j)c_j(t-\tau_j) \\
&\qquad\qquad \times c_i(t-\tau_i)cos(\phi_j-\phi_i)\}dt
\end{aligned} \tag{5.5}$$

where the first term is the information of the ith user, while the other term is the interference from other users. If the perfect time synchronization is achieved, i.e., $\tau_1 = \tau_2 = \cdots = \tau_i = \cdots = \tau_k = \tau$, Eq. (5.5) can be converted into

$$\begin{aligned}
&\int_{\tau_i}^{T+\tau_i} U_i(t)dt = \int_{\tau}^{T+\tau} U_i(t)dt \\
&\approx \frac{1}{2}A_i T d_i + \frac{1}{2}\sum_{\substack{j=1 \\ j\neq i}}^{k} \int_{\tau}^{T+\tau} \{A_j d_j(t-\tau)c_j(t-\tau)\times c_i(t-\tau)\times 1\}dt \\
&= \frac{1}{2}A_i T d_i
\end{aligned} \tag{5.6}$$

where only the data of the ith user is retained, while the interference from other users is eliminated.

5.3 *ConScatter* sequences

Definition. *ConScatter* sequences are defined as a set of N sequences in which each sequence takes on the values $+1$ and -1. *ConScatter* sequences can be generated iteratively. The illustration of generating *ConScatter* codes is shown in Eq. (5.7), where φ^i represents the number of rows in $\mathbb{H}_i$, and $\mathbb{H}_i(j,:)$ denotes all the elements in the jth row of $\mathbb{H}_i$, such as $\mathbb{H}_1(1,:) = \{1\ 1\}$. Each row in $\mathbb{H}_n$ corresponds to an *ConScatter* sequence.

$$\mathbb{H}_1 = \begin{bmatrix} 1 & 1 \\ 1 & -1 \end{bmatrix}, \quad \mathbb{H}_n = \begin{bmatrix} \mathbb{H}_{n-1}(1,:) & \mathbb{H}_{n-1}(1,:) \\ \vdots & \vdots \\ \mathbb{H}_{n-1}(\varphi^{n-1},:) & \mathbb{H}_{n-1}(\varphi^{n-1},:) \\ \mathbb{H}_{n-1}(1,:) & -\mathbb{H}_{n-1}(1,:) \end{bmatrix} (n \geq 2) \tag{5.7}$$

Property. *Any sequence in $\mathbb{H}_n$ is orthogonal not only to other sequences in $\mathbb{H}_n$, but also to the time-shifted versions of those sequences, i.e., $\int_0^T w_i(t) \cdot w_j(t)dt = 0$ and $\int_0^T w_i(t) \cdot w_j(t-\tau_j)dt = 0$ $(i \neq j)$ where w_i and w_j are two different ConScatter codes, T is the spreading code duration, and τ_j is the time delay.*

Proof. Proving the above *Property* is equivalent to proving the following two sub-properties.

- *Sub-property 1. Any sequence in $\mathbb{H}_n$ is orthogonal to other sequences in $\mathbb{H}_n$.*
- *Sub-property 2. Any sequence in $\mathbb{H}_n$ is orthogonal to the time-shifted versions of other sequences in $\mathbb{H}_n$.*

Sub-property 1 and *Sub-property 2* can be proved by mathematical induction as follows. We denote m and w_i^n as the number of rows in $\mathbb{H}_n$ and the ith row code of $\mathbb{H}_n$, respectively. Thus, we obtain $m = \varphi^n = \varphi^{n-1} + 1$. First, we prove *Sub-property 1*. Since $\int_0^T w_i^1(t) \cdot w_j^1(t)dt = 0(i \neq j)$, $\mathbb{H}_1$ satisfies *Sub-property 1*. Assuming that $\mathbb{H}_{n-1}$ satisfies *Sub-property 1*, we have $\int_0^T w_i^{n-1}(t) \cdot w_j^{n-1}(t)dt = 0(i \neq j)$. Thus, we obtain

$$\begin{aligned} &\int_0^T w_i^n(t) \cdot w_j^n(t)dt \\ &= \begin{cases} 2\int_0^T w_i^{n-1}(t) \cdot w_j^{n-1}(t)dt = 0 \ \ (i \neq j \ and \ i, j \neq m) \\ \int_0^T (w_i^{n-1}(t) + (-1)w_i^{n-1}(t))dt = 0 \ \ (i \neq j \ and \ j = m) \end{cases} \end{aligned} \tag{5.8}$$

As a result, we proved that $\mathbb{H}_n$ also satisfies *Sub-property 1*. Next, we prove *Sub-property 2*. Since $\int_0^T w_i^1(t) \cdot w_j^1(t - \tau_j)dt = 0(i \neq j)$, $\mathbb{H}_1$ satisfies *Sub-property 2*. Assuming that $\mathbb{H}_{n-1}$ satisfies *Sub-property 2*, we have $\int_0^T w_i^{n-1}(t) \cdot w_j^{n-1}(t - \tau_j)dt = 0(i \neq j)$. Thus, we obtain

$$\begin{aligned} &\int_0^T w_i^n(t) \cdot w_j^n(t - \tau_j)dt \\ &= \begin{cases} 2\int_0^T w_i^{n-1}(t) \cdot w_j^{n-1}(t - \tau_j)dt = 0 \ \ (i \neq j \ and \ i, j \neq m) \\ \int_0^T w_i^n(t) \cdot w_m^n(t - \tau_m)dt = \int_0^T w_i^n(t - \tau_i) \cdot w_m^n(t)dt \\ = \int_0^T (w_i^{n-1}(t - \tau_i) + (-1)w_i^{n-1}(t - \tau_i))dt = 0 \ (i \neq j \ and \ j = m) \end{cases} \end{aligned} \tag{5.9}$$

As a result, we proved that $\mathbb{H}_n$ also satisfies *Sub-property 2*, thereby proving the above *Property*.

5.4 *ConScatter* Design

5.4.1 Overview

ConScatter is composed of three components: i) a transmitter, ii) k tags, and iii) a receiver, as shown in Fig. 5.4. The transmitter generates an OOK modulated single-frequency signal to serve as the excitation signal and to power the tags. The excitation

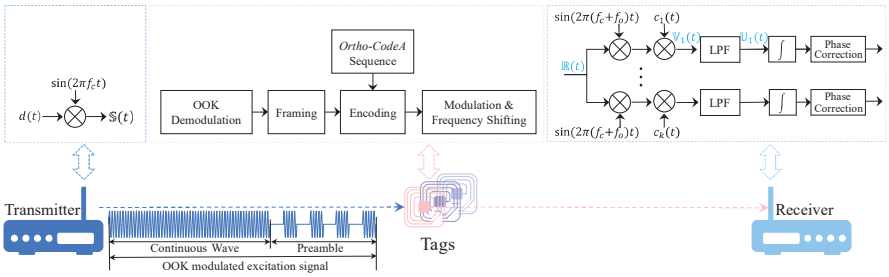

Fig. 5.4 The system overview of *ConScatter*.

signal contains two parts: i) *preamble* and ii) *continuous wave*. The preamble is used for activating the transmission of multiple tags while the continuous wave serves as the backscattered carrier. After identifying such preamble, the tags reflect and modulate the continuous wave to transmit their information. At the receiver, a series of operations are performed to decode the information from the tags.

5.4.2 Transmitter

Produce OOK modulated excitation signal. The main procedure of generating OOK modulated excitation signal is shown at the top-left of Fig. 5.4. Specifically, the transmitter prestores a sequence of $\{1010101011\cdots1\}$ and uses the sequence to modulate a single-frequency carrier signal $sin(2\pi f_c t)$. As a result, we can produce the desired OOK modulated single-frequency signal, which can be mathematically expressed as

$$\mathbb{S}(t) = Ad(t)sin(2\pi f_c t) \tag{5.10}$$

where A, $d(t)$, and f_c are the signal amplitude, the prestored bits of $\{1010101011\cdots1\}$, and the carrier frequency, respectively.

5.4.3 Backscatter tag

The backscatter tag is first triggered by the OOK modulated excitation signal. Then, it performs OOK demodulation to check the preamble in the signal. Once the decoded preamble matches a predefined sequence of $\{10101010\}$, the tag performs the following operations including framing, encoding, modulation, and frequency shifting.

- *OOK demodulation.* We refer to the demodulation module design in [6, 18], in which an analog envelope detector and a comparator are used to decode the OOK modulated signal.

- *Framing.* The information to be transmitted is first encapsulated into frames with the two fields, i) one byte preamble and ii) up to 29 bytes of payload data. The preamble consists of a known sequence of all ones, which serves as a reference symbol to assist in decoding at the receiver. The detailed description involving the preamble is presented in Subsection 5.4.4.
- *Encoding.* The data encapsulated in frames is then encoded using a preassigned *ConScatter* sequence. An example to illustrate the encoding process is as follows. Given an *ConScatter* sequence $\{1\ 1\ -1\ -1\}$, if the input bit is one, the resulting data through the encoding process is "11-1-1". If the input bit is zero, the resulting data is "-1-111".
- *Modulation and frequency shifting. ConScatter* tags adopt BPSK modulation. Specifically, if the bit being transmitted is '-1', then the tag introduces a phase shift of 180 degrees in the backscattered signal. If the bit being transmitted is '1', no phase shift is introduced. To reduce the interference from the excitation signal, the tag shifts the backscattered signal by 20 MHz in our system. The frequency shifting operation uses the same technique as in [34].

Let τ_{ti} be the propagation delay from the transmitter to the ith tag. The incoming excitation signal for the ith tag, denoted by $\mathbb{R}_{ti}(t)$, can be written as

$$\mathbb{R}_{ti}(t) = A_{ti}d(t-\tau_{ti})sin(2\pi f_c(t-\tau_{ti})) \tag{5.11}$$

where A_{ti} is the amplitude, and we neglect noise for simplicity. After modulation and frequency shifting operations, the backscattered signal can be represented as

$$\mathbb{B}_i(t) = A_{ti}^{'}d_i(t)c_i(t)sin(2\pi(f_c+f_o)(t-\tau_{ti})) \tag{5.12}$$

where $A_{ti}^{'}$, $d_i(t)$, $c_i(t)$, and f_o are the backscattered signal amplitude, information bits, spreading signal, and shifting frequency for the ith tag, respectively. The shifting frequency f_o is the same for all tags.

5.4.4 Receiver

The main procedure of the receiver is shown at the top-right of Fig. 5.4. Let τ_{ir} be the propagation delay from the ith tag to the receiver. We describe the received signal only for the noise channel. Thus, the received signal at the receiver can be expressed as

$$\begin{aligned}\mathbb{R}(t) &= \sum_{i=1}^{k} A_{ir}d_i(t-\tau_{ir})c_i(t-\tau_{ir})sin(2\pi(f_c+f_o)(t-\tau_{ti}-\tau_{ir}))+n(t)\\ &= \sum_{i=1}^{k} A_{ir}d_i(t-\tau_{ir})c_i(t-\tau_{ir})sin(2\pi(f_c+f_o)t+\phi_i)+n(t)\end{aligned} \tag{5.13}$$

where $\phi_i = -2\pi(f_c+f_o)(\tau_{ti}+\tau_{ir})$. *ConScatter* is able to decode the ith tag data without the need for phase synchronization. Specifically, after multiplying $\mathbb{R}(t)$ by $sin(2\pi(f_c+f_o)t)$ and $c_i(t)$, the received signal becomes

$$
\begin{aligned}
&\mathbb{V}_i(t) = \mathbb{R}(t) \times sin(2\pi(f_c + f_o)t) \times c_i(t) \\
&= \left\{ \sum_{i=1}^{k} A_{ir} d_i(t - \tau_{ir}) c_i(t - \tau_{ir}) sin(2\pi(f_c + f_o)t + \phi_i) + n(t) \right\} \\
&\qquad\qquad \times sin(2\pi(f_c + f_o)t) \times c_i(t) \\
&= \frac{1}{2} A_{ir} d_i(t - \tau_{ir}) c_i(t - \tau_{ir}) c_i(t) (cos\phi_i - cos(4\pi(f_c + f_o)t + \phi_i)) \\
&\quad + \frac{1}{2} \sum_{\substack{j=1 \\ j \neq i}}^{k} \{ A_{jr} d_j(t - \tau_{jr}) c_j(t - \tau_{jr}) c_i(t) \\
&\qquad\qquad \times (cos(\phi_j) - cos(4\pi(f_c + f_o)t + \phi_j)) \} \\
&\quad + n(t) sin(2\pi(f_c + f_o)t) c_i(t)
\end{aligned} \tag{5.14}
$$

The $\mathbb{V}_i(t)$ at the output of the LPF is converted to

$$
\begin{aligned}
\mathbb{U}_i(t) = &\frac{1}{2} A_{ir} d_i(t - \tau_{ir}) c_i(t - \tau_{ir}) c_i(t) cos\phi_i \\
&+ \frac{1}{2} \sum_{\substack{j=1 \\ j \neq i}}^{k} \{ A_{jr} d_j(t - \tau_{jr}) c_j(t - \tau_{jr}) c_i(t) cos(\phi_j) \}
\end{aligned} \tag{5.15}
$$

After passing through the integrator, the $\mathbb{U}_i(t)$ becomes

$$
\begin{aligned}
\int_0^T \mathbb{U}_i(t) dt = &\int_0^T \frac{1}{2} A_{ir} d_i(t - \tau_{ir}) c_i(t - \tau_{ir}) c_i(t) cos\phi_i dt \\
&+ \int_0^T \sum_{\substack{j=1 \\ j \neq i}}^{k} \frac{1}{2} A_{jr} d_j(t - \tau_{jr}) c_j(t - \tau_{jr}) c_i(t) cos\phi_j dt
\end{aligned} \tag{5.16}
$$

Because *ConScatter* codes have the property of $\int_0^T c_i(t) c_j(t - \tau_{jr}) = 0$ $(i \neq j)$, Eq. (5.16) can be rewritten as

$$
\begin{aligned}
\int_0^T \mathbb{U}_i(t) dt &= \int_0^T \frac{1}{2} A_{ir} d_i(t - \tau_{ir}) c_i(t - \tau_{ir}) c_i(t) cos\phi_i dt \\
&= \frac{1}{2} A_{ir} \int_0^T d_i(t - \tau_{ir}) c_i(t - \tau_{ir}) c_i(t) cos\phi_i dt
\end{aligned} \tag{5.17}
$$

We evaluate the impact of τ_{ir} on the $\int_0^T c_i(t - \tau_{ir}) c_i(t) dt$, as shown in Fig. 5.5.

The results show that the polarity of the value $\int_0^T c_i(t - \tau_{ir}) c_i(t) dt$ changes with the change of τ_{ir} and is constant when $0 < \tau_{ir} < 0.5T_c$. Given that $0 < \tau_{ir} < 0.5T_c$, Eq. (5.17) will be approximately equal to

$$
\int_0^T \mathbb{U}_i(t) dt \approx \frac{1}{2} A_{ir} \rho_i cos\phi_i d_i \tag{5.18}
$$

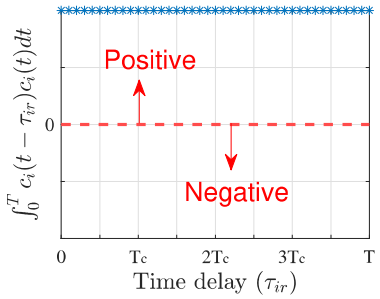

(a) The *ConScatter* code used is {1111}.

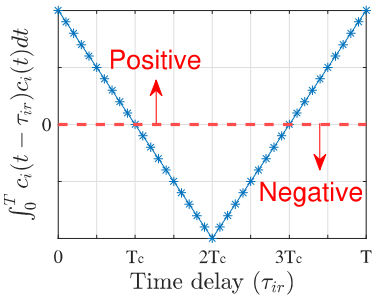

(b) The *ConScatter* code used is {11−1−1}.

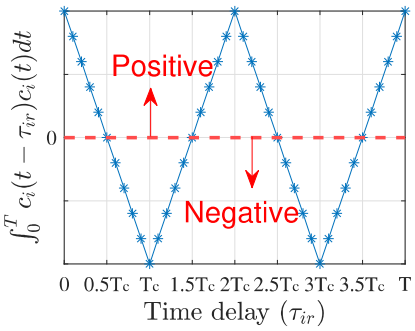

(c) The *ConScatter* code used is {1−11−1}.

Fig. 5.5 The value of $\int_0^T c_i(t-\tau_{ir})c_i(t)dt$ varying τ_{ir}, in which T_c is the duration of a chip (i.e., a spreading bit).

where ρ_i is a positive number. From Eq. (5.18), we conclude that if the $cos\phi_i$ can be efficiently addressed, we will have the opportunity to correctly demodulate the ith tag data. This is because $cos\phi_i \in [-1, 1]$, thus the decoded bit may be the opposite of the original transmitted bit. For example, the transmitted bit is '1' while the decoded bit is '-1'. To address this problem, we propose a reference-based symbol scheme. Specifically, the tag i transmits a sequence of all ones before transmitting data, i.e, the preamble field in frames mentioned in Subsection 5.4.3. At the receiver, we use the known sequences of all ones to eliminate the impact of $cos\phi_i$.

Frequency Mismatch. While our system works well in principle, an issue arises in practice, i.e., the device experiences the frequency offset [15, 16]. The change in frequency may have a negative impact on the resulting demodulation, thereby causing a high BER. We test the impact of the frequency offset on the system performance, as shown in Fig. 5.6. We can conclude that the maximum frequency offset tolerated by *ConScatter* is 132 Hz. However, the practical frequency offset may exceed 132 Hz. To address this issue, we use a frequency compensator to compensate for the frequency offset. The frequency compensator uses FFT-based algorithms to estimate the frequency offset. More details about the algorithm can be found in [35]. The result

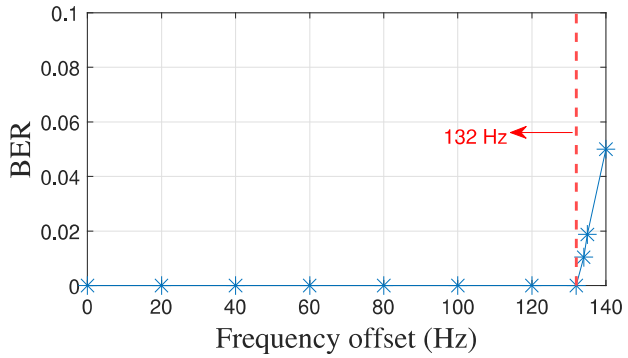

Fig. 5.6 The BER for different frequency offset evaluation.

of evaluating the frequency compensator varying the frequency offset is depicted in Fig. 5.7. We can see that the frequency compensator is able to compensate for the frequency offset, thus mitigating the effect of the frequency offset.

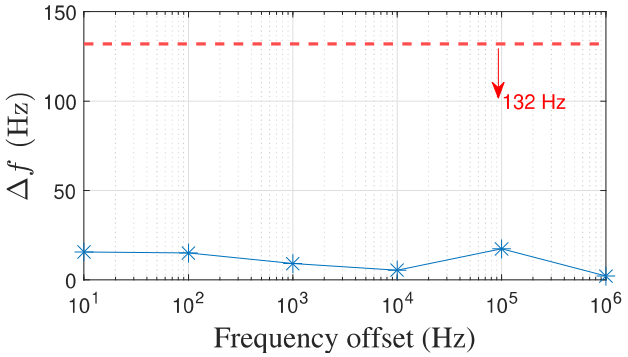

Fig. 5.7 The frequency difference (denoted by Δf) after using the frequency compensator, in which the frequency difference is the difference between the actual frequency and the measured frequency.

5.5 Simulations

5.5.1 Simulation setup

The performance of *ConScatter* is evaluated using MATLAB R2021a. We place a transmitter, a group of tags, and a receiver in an indoor environment with a size of $8m \times 5m \times 3m$. The indoor simulation environment is an office 3-D map which is

an STL format file provided by MATLAB. We specify the surface material of the scene as plasterboard. Ray tracing [36] is used to build multipath fading channel and analyze multi-path effects, which is a channel model that has been frequently used for RF signals analysis and can accurately describe the multi-path effect for a given indoor environment model [37]. The transmitter operates at a carrier frequency of 2 GHz with a power level of 30 dBm. The frequency shifting f_o introduced by the tag is set to 20 MHz. Unless otherwise specified, the number of tags is set to 2; the signal-to-noise ratio (SNR), the maximum number of path reflections [4], and the duration of each spreading bit are set to 10 dB, 1, and 0.5 μs, respectively. The duration is sufficient for such an indoor environment.

5.5.2 Simulation results

5.5.2.1 OOK demodulation

We first study the performance of the OOK demodulation module in our system. In this simulation, a group of 50 tags are randomly deployed in the office 3-D map environment. The results of evaluating OOK identification accuracy varying SNR are depicted in Fig. 5.8. The results show that the identification accuracy reaches 99% when SNR is greater than −3 dB.

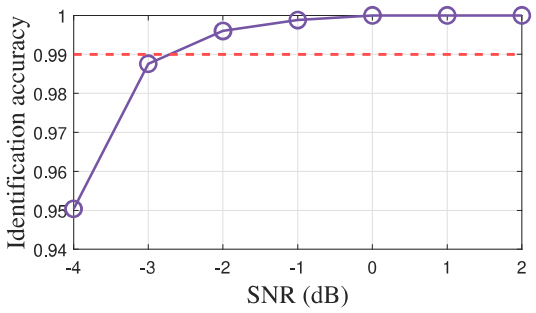

Fig. 5.8 OOK demodulation accuracy varying SNR.

5.5.2.2 Impact of SNR

In this scenario, we intentionally let the tag performs the backscatter operation, regardless of the result of OOK demodulation, to comprehensively measure the

[4] The maximum number of path reflections refers to the maximum number of reflections the backscattered signal experiences before reaching the receiver.

impact of SNR on the BER of *ConScatter*. We vary SNR from -14 to 2 dB and the number of concurrent tags changes from 2 to 3. The results are depicted in Fig. 5.9. We can see that the BER decreases with the increment of SNR, and that there is no significant BER difference for 2 tags and 3 tags. In addition, the results show that we achieve BER of 0 when SNR is greater or equal to -8 dB owing to the following two reasons. On the one hand, *ConScatter* uses spread spectrum technique that can suppress the noise and be resistant to noise, thus minimizing the effect of the noise. On the other hand, our system adopts *ConScatter* sequences. Thus, the orthogonality among spreading sequences can be maintained, thereby minimizing or even eliminating the interference from other tags.

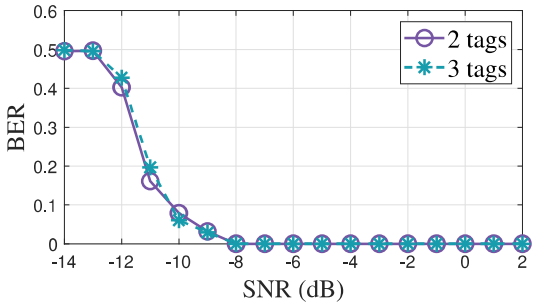

Fig. 5.9 Impact of SNR.

5.5.2.3 Impact of frequency offsets

Next, we evaluate the impact of frequency offsets on the BER of *ConScatter* by varying frequency offsets from 10^1 to 10^6 Hz. We compare the performance of our system, both with and without frequency compensator (denoted by *with f-c* and *without f-c*), as shown in Fig. 5.10. The results show that the BER without frequency compensator is much higher than that with frequency compensator, and that the system with frequency compensator achieves BER of 0. The main reason is that the frequency compensator can compensate for the frequency offset and reduce the frequency difference to a tolerable range (see Fig. 5.7), thereby achieving BER of 0.

5.5.2.4 Impact of maximum number of path reflections

Now, we vary the maximum number of path reflections from 1 to 5 to evaluate the performance of *ConScatter* regarding BER. The results demonstrate that *ConScatter* achieves BER of 0 due to the following two reasons. First, the tag data is encoded using spreading sequences, thus resulting in the backscattered signals with a large bandwidth and distributing the power of those signals over the whole bandwidth.

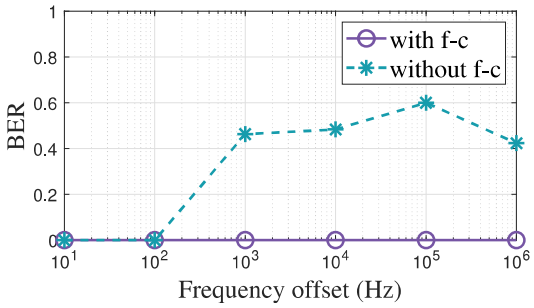

Fig. 5.10 Impact of frequency offsets.

As a result, only a small portion of the entire signal is affected by multipath fading. Second, our system uses *ConScatter* codes, in which any code is orthogonal not only to other codes but also to the time-shifted versions of those codes, thereby maintaining the orthogonality among codes and minimizing the interference from other tags.

5.5.2.5 Concurrency and capacity

In this scenario, we evaluate the concurrency and capacity of our system. The results are illustrated in Fig. 5.11 and Fig. 5.12. We can observe that our system can support concurrent transmissions of up to 7 tags with BER of 0, and the corresponding network capacity (i.e., aggregate throughput) varies from 218.7 Kbps to 1.5 Mbps. In addition, we can see that the BER rises to the level of 10^{-1} and the aggregate throughput drops to the level of 100 Kbps when the number of concurrent tags reaches 8. This is reasonable since the length of *ConScatter* sequences used by tags increases as the number of concurrent tags increases. As a result, the number of valid bits transmitted decreases accordingly, thereby leading to a reduction in the capacity. In addition, the increment in the length of spreading sequences also inevitably leads to an extension in the signal transmission time. As a result, a low frequency difference Δf also leads to a rise in BER.

5.5.2.6 Comparison with the existing work

To prove the benefit of *ConScatter*, we implement the μcode [38], which is a well-known concurrent transmission method using coding mechanisms, as our baseline. In this scenario, we vary SNR from 0 to 15 dB and the number of concurrent tags is set to 2. In our simulation of μcode, the chip length (denoted by L) is set at 16 and 48, which is the same for the two tags; the two tags transmit at chip rates of 10 Mchips/s and 20 Mchips/s, respectively. The results are shown in Fig. 5.13. We can see that *ConScatter* achieves BER of 0 for the same reasons explained in Subsection 5.5.2.2,

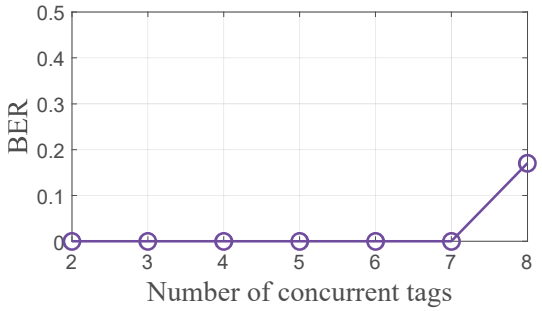

Fig. 5.11 Concurrency evaluation.

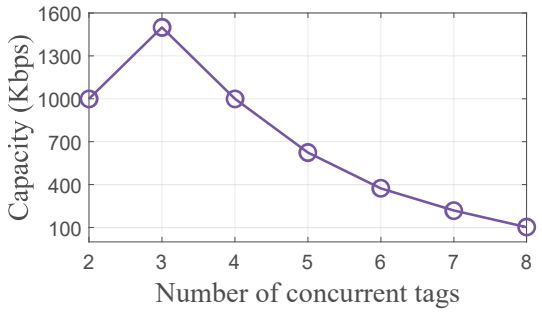

Fig. 5.12 Capacity evaluation.

and that SNR has a slight impact on BER since spread-spectrum communication is resistant to noise. In addition, we can observe that *ConScatter* achieves lower BER than μcode. The main reason is the use of *ConScatter* codes, which can maintain the orthogonality among codes, thus minimizing the interference from other tags.

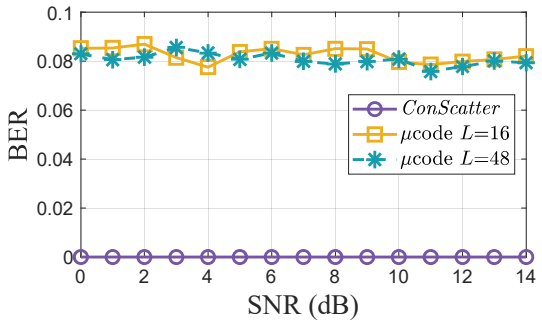

Fig. 5.13 Comparison with μcode [38].

5.6 Related Work

As a passive communication solution, backscatter communication has been a popular research field. In this paper, we present a backscatter multiple access scheme that targets indoor IoT applications. Our work is inspired by the recent studies in [6, 15, 16, 18, 19, 32, 34, 38–40], which are discussed as follows.

Low-power demodulator at tags. Liu *et al.* [6] present a novel demodulator design. The demodulator runs on the tag side and is able to decode OOK modulated signals in an ultra-low-power manner. Zhang *et al.* [18] use an analog envelope detector to decode OOK modulated signals on the tag side. This envelope detector uses a threshold to distinguish between bit '0' and bit '1'. Our work is based on the demodulation module design in the above two studies.

Self-interference cancellation. The excitation signal may interfere with the backscattered signal when they share the same frequency band, thereby causing decoding errors. Zhang *et al.* [40] propose a frequency-shifted backscatter technique, which allows tags to shift the backscattered signal to a non-overlapping frequency band while consuming tens of micro-watts, thereby reducing self-interference. However, the frequency shifting technique in [40] creates copies on both sides of the excitation signal, thus leading to unwanted interference in other band. The studies in [18, 34] resolve the double side-band backscatter problem and present the single side-band backscatter design. Our work borrows the frequency shifting design in [34].

Backscatter multiple access. Most of the existing backscatter multiple access schemes [19] are based on the *Frame Slotted Aloha*, in which the information of each tag is transmitted at different slots, thereby leading to the inefficiency. The work in [39] supports the transmissions from 2 tags in sequence by allocating different data fields in one packet to different tags. The studies in [15, 16, 32, 38] support concurrent transmissions from multiple tags. However, these schemes are not designed specifically for particular applications and fail to consider the practical application requirements.

In summary, inspired by the above studies, we present *ConScatter*, a backscatter multiple access scheme that targets indoor IoT applications, such as the smart home, and contemplates the practical application requirements. The theoretical analysis and extensive evaluations confirm the effectiveness of our scheme.

5.7 Discussion and conclusion

In this paper, we propose *ConScatter*, a backscatter multiple access scheme that supports concurrent transmissions from multiple tags and targets indoor IoT applications. To implement *ConScatter*, the key challenges such as imperfect time synchronization, high hardware complexity at receiver, and coordinating multiple tags have been addressed. However, our work also faces some limitations.

Limited number of concurrent tags. While the simulation results show that *ConScatter* supports concurrent transmissions of up to 7 tags, the results are below the theoretical expectation (i.e., at least 9 tags if the length of codes exceeds 256). We explained the reasons for this phenomenon in Subsection 5.5.2.5. A potential solution is to periodically insert reference symbols into the transmitted data. The receiver leverages these reference symbols to correct bit errors incurred by the frequency difference. We leave the implementation of such a solution to future work.

Deployment of a dedicated carrier emitter. The current *ConScatter* design uses a dedicated carrier emitter to produce a single-tone signal as the excitation signal. This may increase the cost compared to the studies using existing ambient signals (e.g., Wi-Fi, LoRa, and Bluetooth) as the excitation signal. The work in [34] has demonstrated that Bluetooth radios can be used to produce the single-tone signal, which provides *ConScatter* the opportunity to use Bluetooth radios as carrier emitters. We leave such an implementation to future work.

Real-world validation. For the moment, our work is evaluated and validated by theoretical analysis and simulation evaluation. Some practical factors (e.g., intermittent operation) may degrade the performance of *ConScatter*. One possible solution is to view the intermittent operation as an undesirable operation. Specifically, when the intermittent operation occurs, the tag will stop the current backscatter operation until the next excitation signal arrives. We leave the real-world validation to future work.

References

1. Harry Stockman. Communication by means of reflected power. *Proc. of IEEE IRE*, 1948.
2. Nguyen Van Huynh, Dinh Thai Hoang, Xiao Lu, Dusit Niyato, Ping Wang, and Dong In Kim. Ambient backscatter communications: A contemporary survey. *IEEE Communications surveys & tutorials*, 20(4):2889–2922, 2018.
3. Weiqi Wu, Xingfu Wang, Ammar Hawbani, Longzhi Yuan, and Wei Gong. A survey on ambient backscatter communications: Principles, systems, applications, and challenges. *Computer Networks*, page 109235, 2022.
4. Mudasar Latif Memon, Navrati Saxena, Abhishek Roy, and Dong Ryeol Shin. Backscatter communications: Inception of the battery-free era—a comprehensive survey. *Electronics*, 8(2):129, 2019.
5. Zhaoyuan Xu and Wei Gong. Enabling zigbee backscatter communication in a crowded spectrum. In *Proc. IEEE ICNP*, 2022.
6. Vincent Liu, Aaron Parks, Vamsi Talla, Shyamnath Gollakota, David Wetherall, and Joshua R Smith. Ambient backscatter: Wireless communication out of thin air. *Proc. of ACM SIGCOMM*, 2013.
7. Wei Gong, Longzhi Yuan, Qiwei Wang, and Jia Zhao. Multiprotocol backscatter for personal iot sensors. In *Proc. of ACM CoNEXT*, 2020.
8. Wei Gong, Si Chen, and Jiangchuan Liu. Towards higher throughput rate adaptation for backscatter networks. In *Proc. IEEE ICNP*, 2017.
9. Wei Gong, Si Chen, Jiangchuan Liu, and Zhi Wang. Mobirate: Mobility-aware rate adaptation using phy information for backscatter networks. In *Proc. IEEE INFOCOM*, 2018.
10. Wei Gong, Ivan Stojmenovic, Amiya Nayak, Kebin Liu, and Haoxiang Liu. Fast and scalable counterfeits estimation for large-scale rfid systems. *IEEE/ACM transactions on networking*, 24(2):1052–1064, 2015.

11. Wei Gong, Jiangchuan Liu, and Zhe Yang. Fast and reliable unknown tag detection in large-scale rfid systems. In *Proc. of ACM/IEEE MobiHoc*, 2016.
12. Haoxiang Liu, Wei Gong, Xin Miao, Kebin Liu, and Wenbo He. Towards adaptive continuous scanning in large-scale rfid systems. In *Proc. IEEE INFOCOM*, 2014.
13. Wei Gong, Haoxiang Liu, Kebin Liu, Qiang Ma, and Yunhao Liu. Exploiting channel diversity for rate adaptation in backscatter communication networks. In *Proc. IEEE INFOCOM*, 2016.
14. Wei Gong, Haoxiang Liu, Jiangchuan Liu, Xiaoyi Fan, Kebin Liu, Qiang Ma, and Xiaoyu Ji. Channel-aware rate adaptation for backscatter networks. *IEEE/ACM Transactions on Networking*, 26(2):751–764, 2018.
15. Mehrdad Hessar, Ali Najafi, and Shyamnath Gollakota. Netscatter: Enabling large-scale backscatter networks. In *Proc. USENIX NSDI*, 2019.
16. Renjie Zhao, Fengyuan Zhu, Yuda Feng, Siyuan Peng, Xiaohua Tian, Hui Yu, and Xinbing Wang. Ofdma-enabled wi-fi backscatter. In *Proc. of ACM MobiCom*, 2019.
17. Yifan Yang and Wei Gong. Universal space-time stream backscatter with ambient wifi. In *Proc. IEEE PERCOM*, 2022.
18. Pengyu Zhang, Dinesh Bharadia, Kiran Joshi, and Sachin Katti. Hitchhike: Practical backscatter using commodity wifi. In *Proc. of ACM SenSys*, 2016.
19. Pengyu Zhang, Colleen Josephson, Dinesh Bharadia, and Sachin Katti. Freerider: Backscatter communication using commodity radios. In *Proc. of ACM CoNEXT*, 2017.
20. Yifan Yang, Longzhi Yuan, Jia Zhao, and Wei Gong. Content-agnostic backscatter from thin air. In *Proc. of ACM MobiSys*, 2022.
21. Xin Liu, Zicheng Chi, Wei Wang, Yao Yao, and Ting Zhu. Vmscatter: A versatile mimo backscatter. In *Proc. USENIX NSDI*, 2020.
22. Cdma. https://en.wikipedia.org/wiki/Code-division_multiple_access.
23. Spread spectrum. https://en.wikipedia.org/wiki/Spread_spectrum.
24. The advantages of the spread spectrum technique. https://resources.system-analysis.cadence.com/blog/msa2022-the-advantages-of-the-spread-spectrum-technique.
25. Andrea Goldsmith. *Wireless communications*. Cambridge university press, 2005.
26. Si-Yue Sun, Hsiao-Hwa Chen, and Wei-Xiao Meng. A survey on complementary-coded mimo cdma wireless communications. *IEEE Communications Surveys & Tutorials*, 17(1):52–69, 2014.
27. Ramjee Prasad and Tero Ojanpera. An overview of cdma evolution toward wideband cdma. *IEEE communications Surveys*, 1(1):2–29, 1998.
28. Andrew J Viterbi. *CDMA: principles of spread spectrum communication*. Addison Wesley Longman Publishing Co., Inc., 1995.
29. Esmael H Dinan and Bijan Jabbari. Spreading codes for direct sequence cdma and wideband cdma cellular networks. *IEEE communications magazine*, 36(9):48–54, 1998.
30. Cdma tutorial. https://www.tutorialspoint.com/cdma/cdma_quick_guide.htm.
31. Cdma orthogonal spreading codes. https://www.electronics-notes.com/articles/radio/dsss/cdma-orthogonal-spreading-codes.php.
32. Carlo Mutti and Christian Floerkemeier. Cdma-based rfid systems in dense scenarios: Concepts and challenges. In *Proc. IEEE RFID*, 2008.
33. Enrique Garcia, José A Paredes, Fernando J Álvarez, M Carmen Pérez, and Juan Jesús García. Spreading sequences in active sensing: A review. *Signal Processing*, 106:88–105, 2015.
34. Vikram Iyer, Vamsi Talla, Bryce Kellogg, Shyamnath Gollakota, and Joshua Smith. Inter-technology backscatter: Towards internet connectivity for implanted devices. In *Proc. of ACM SIGCOMM*, 2016.
35. Yan Wang, Kai Shi, and Erchin Serpedin. Non-data-aided feedforward carrier frequency offset estimators for qam constellations: A nonlinear least-squares approach. *EURASIP journal on advances in signal processing*, 2004(13):1–9, 2004.
36. Zhengqing Yun and Magdy F Iskander. Ray tracing for radio propagation modeling: Principles and applications. *IEEE access*, 3:1089–1100, 2015.
37. Danping He, Bo Ai, Ke Guan, Longhe Wang, Zhangdui Zhong, and Thomas Kürner. The design and applications of high-performance ray-tracing simulation platform for 5g and beyond wireless communications: A tutorial. *IEEE Communications Surveys & Tutorials*, 21(1):10–27, 2018.

38. Aaron N Parks, Angli Liu, Shyamnath Gollakota, and Joshua R Smith. Turbocharging ambient backscatter communication. *Proc. of ACM SIGCOMM*, 2014.
39. Jia Zhao, Wei Gong, and Jiangchuan Liu. X-tandem: Towards multi-hop backscatter communication with commodity wifi. In *Proc. of ACM MobiCom*, 2018.
40. Pengyu Zhang, Mohammad Rostami, Pan Hu, and Deepak Ganesan. Enabling practical backscatter communication for on-body sensors. In *Proc. of ACM SIGCOMM*, 2016.